





Toughness-drop in AISI 316L pipe after service exposure at 720 °C for 100,700 hours

Flavio Pereira de Moraes¹ 
Emanuelle Machado Amaral^{1*} 
Flávio Beneduce Neto¹ 
Angelo Fernando Padilha¹ 

Abstract

AISI 316L austenitic stainless steel pipes employed in a petrochemical industry for 100,700 hours at 720 °C were examined in this study. During this exposure, the microstructure changed significantly, and the toughness of the pipe decreased dramatically. Detailed microstructural analyses revealed that although several phases precipitated during service, sigma phase precipitation at the grain boundaries was primarily responsible for the observed decrease in toughness. Nonetheless, the decreased toughness did not hinder the operation of the pipes until the anticipated deadline of the project.

Keywords: AISI 316L; Pipes; Sigma phase; Toughness-drop.

Queda de tenacidade em tubulação de AISI 316L após exposição em serviço a 720 °C por 100.700 horas

Resumo

Tubulação de aço inoxidável austenítico AISI 316L foi utilizada em uma indústria petroquímica por 100.700 horas a 720 °C. Durante esta exposição, a microestrutura do aço mudou significativamente e a tenacidade dos tubos caiu drasticamente. As análises realizadas neste trabalho mostraram que, embora diversas fases tenham precipitado durante a operação, a precipitação da fase sigma nos contornos de grão foi a principal responsável pela queda de tenacidade. Contudo, vale ressaltar que a queda de tenacidade não impediu que as tubulações continuassem normalmente em operação até o prazo limite previsto no projeto.

Palavras-chave: AISI 316L; Tubulação; Fase sigma; Queda de tenacidade.

1 Introduction

Stainless steels constitute approximately 3% of total steel production by weight; however, their share in terms of income is significantly higher. Among the various classes of stainless steels, austenitic steels are the most commonly used owing to their excellent ductility and toughness. While there are several compositions of austenitic stainless steels (ASSs) available in the market, six compositions are particularly prevalent: AISI 304, 304L, 316, 316L, 321, and 347. Among these, 316 and 316L are the most used at high temperatures, ranging between 550 and 750 °C [1]. For instance, solution-annealed 316L steel exhibits an engineering strain exceeding 60% in the tensile test [2] and absorbed energy above 100 Joules in the Charpy impact test at room temperature [3].

Three primary situations, all related to the usage conditions of the material, specifically in 316L steel, can

lead to significant reduction in toughness: i) stress corrosion cracking, examined in a recent paper published by the current authors [4]; ii) neutron irradiation during the operation of nuclear reactors [5-7], which is out of the scope of this paper; and iii) precipitation of deleterious phases during service at high temperatures, which is the central focus of this article.

During high temperature exposure of AISI 316 and 316L steels, two types of carbides rich in chromium and molybdenum ($M_{23}C_6$ and M_6C) along with three intermetallic phases (sigma, chi, and Laves) can precipitate via nucleation and growth involving atomic diffusion [8-17]. Additionally, silicide precipitation, referred to as phase G (owing to its recurrent occurrence at the grain boundaries), is occasionally mentioned [16,17]. Table 1 summarizes the main characteristics that are useful for identifying the aforementioned phases.

¹Departamento de Engenharia Metalúrgica e de Materiais, Escola Politécnica, Universidade de São Paulo, São Paulo, SP, Brasil.

*Corresponding author: emanuelleamaral@usp.br



Table 1. Crystal structure, lattice parameters, and composition (estimated stoichiometry) of carbides and intermetallic phases that precipitate in AISI 316 and 316L steels [17]

Phase	Crystal structure	Typical lattice parameters (nm)	Composition
$M_{23}C_6$	fcc	1.057 – 1.068	$(Fe, Cr, Mo)_{23}C_6$
M_6C	fcc	1.095 – 1.128	$(Fe, Cr, Mo)_6C$
Sigma (σ)	tcc	0.87 – 0.92	$(Fe, Ni)_X(Cr, Mo)_Y$
Chi (χ)	bcc	0.8807 – 0.892	$(Fe, Ni)_{36}Cr_{18}Mo_4$
Laves	hcp	0.473 – 0.474	$(Fe, Ni)_2(Mo, Si)$
G	fcc	1.122 – 1.124	$Ni_{16}Nb_6Si_7; Ni_{16}Ti_6Si_7$

Table 2. Chemical composition (wt.%) of the AISI 316L pipe (average of three analyses)

C	Si	Mn	P	S	Cr	Ni	Co	Mo	Ti	V	Nb	Cu	W	N
0.022	0.342	1.703	0.021	0.020	16.481	11.592	0.089	2.105	0.002	0.049	0.003	0.252	0.064	0.036

According to Johansson and Lind [18], it is likely that in the past, η -nitride (having a diamond cubic structure; Fd3m space group) was indexed as the M_6C carbide and/or as the silicon-containing G phase. Moreover, Maziasz [19] detected the presence of η -nitrides in a batch of 316 austenitic stainless steels containing 0.050 wt.% nitrogen and 0.8 wt.% silicon exposed to thermal aging or irradiation environments.

In general, the precipitation of carbides occurs quickly (in minutes), while the precipitation of intermetallic phases from austenite is slow and requires hundreds or even thousands of hours [8-17], as illustrated in Figure 1.

However, the most common ASSs are not fully austenitic in the solution annealed condition and may contain delta (δ) ferrite between 0.5 and 7 vol% [20-22]. The presence of delta ferrite in the microstructure enables the rapid formation of sigma phase (in a few hours) via eutectoid decomposition: $\delta \rightarrow \sigma + \gamma'$ [23,24].

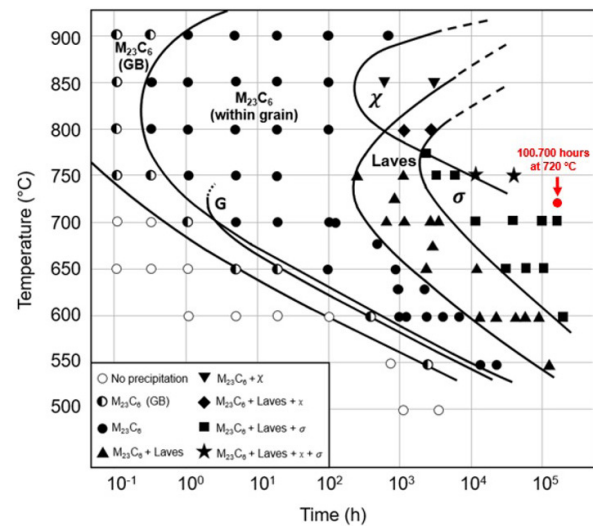
This paper has two main objectives: i) characterize in detail the microstructure of a thick-walled 316LASS pipe used in the petrochemical industry for 100,700 hours at a temperature of 720 °C and ii) evaluate the toughness drop caused by the microstructure modifications.

2 Materials and methods

The results of the chemical analysis of the steel investigated in this study are listed in Table 2.

Charpy impact tests were performed at room temperature using notched specimens with standardized dimensions ($10 \times 10 \times 55$ mm). The Charpy impact test was repeated three times to ensure the reproducibility.

Microstructural characterization was performed using optical microscopy (OM), and scanning electron microscopy (SEM) combined with energy-dispersive spectroscopy (EDS). The metallographic sample preparation comprised grinding, polishing with diamond suspension of 6, 3, and 1 μ m followed by etching, electrolytic and chemical.

**Figure 1.** Time-Temperature-precipitation (TTP) diagram for an AISI 316 steel [15]. The red point indicates the conditions of exposure in the present study.

Electrolytic etching was carried out at 6 V for 10 s using 10% oxalic acid (by volume) and 90% distilled water. Chemical etching was carried out using the V2A reagent solution containing 100 ml H_2O , 100 ml HCl, 10 ml HNO_3 , and 0.3 ml Vogel's special reagent [25].

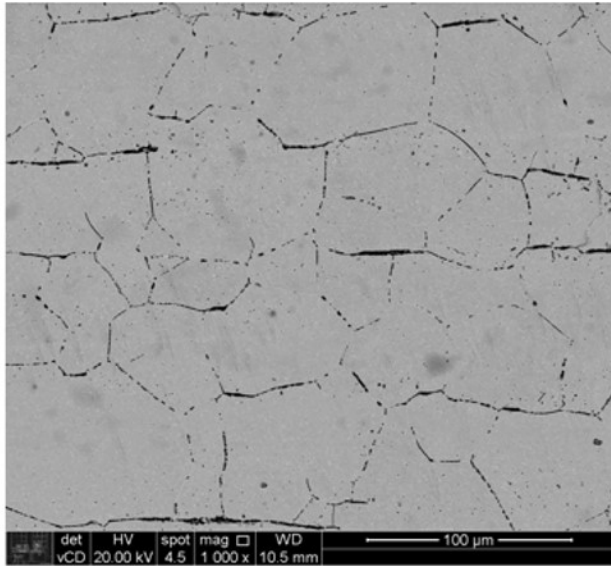
3 Results and discussion

Initially, residual ferromagnetism in the pipe was measured using a ferrite detector with a detection limit of 0.1%. The measurements revealed no detectable delta ferrite. However, prediction of delta ferrite by plotting the chemical composition from Table 2 on the Schaeffler diagram, revealed the presence of delta ferrite. The predicted percentage of delta ferrite (%F) [22] was calculated to be 5.7% using Equation (1).

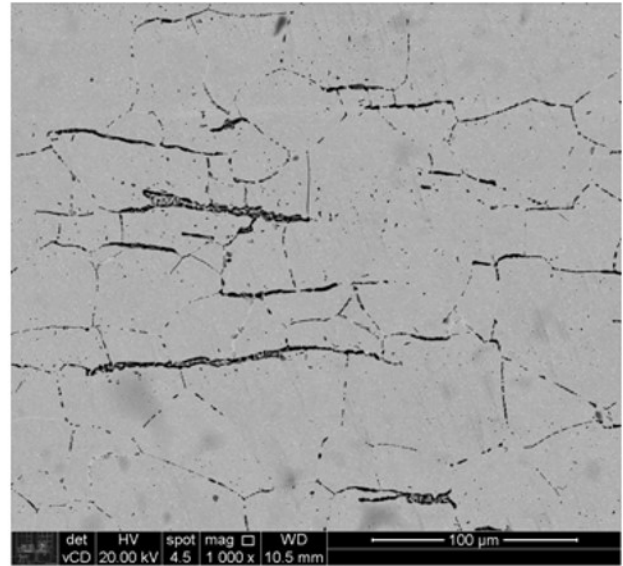
$$\%F = 1.35 Cr + 0.39 Si + 8.8 Mo + 4.01 Ti - 14.78 C - 0.65 Mn - 1.72 Ni - 13.88 \quad (1)$$

Three standardized Charpy tests conducted at room temperature, yielded very low values of 8, 9, and 8 Joules. Subsequently, the microstructure of the cross-section of the Charpy specimens was analyzed (Figure 2).

Figure 2 illustrates precipitation at grain boundaries (Figure 2a) and the presence of transformed delta ferrite stringers ($\delta \rightarrow \sigma + \gamma'$) crossing several grains (Figure 2b). On the other hand, the electrolytic etching using oxalic acid removed most of the precipitates. Figure 3 shows the microstructures obtained after chemical etching using the V2A reagent, preserving the precipitates. The gray

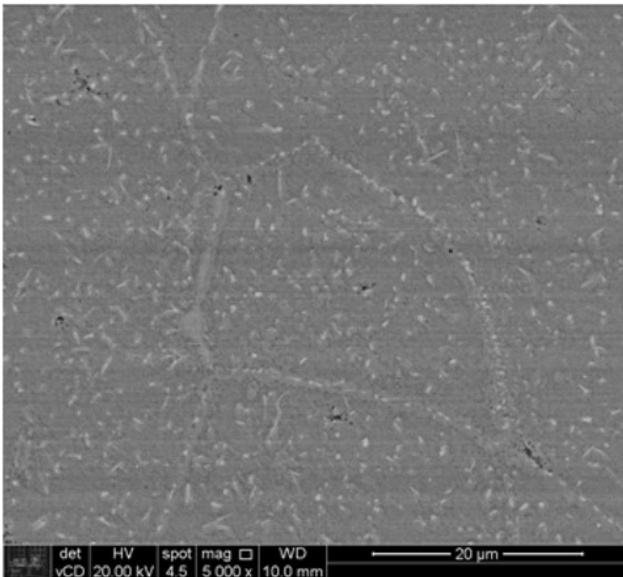


(a)

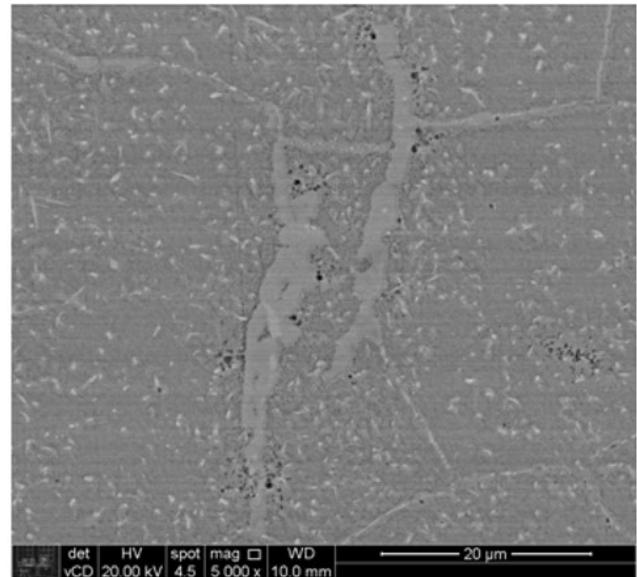


(b)

Figure 2. SEM (a) and (b) images of the cross-section of a Charpy specimen obtained using backscattered electrons after electrolytic etching with 10% oxalic acid solution.



(a)



(b)

Figure 3. SEM (a) and (b) images of the cross-section of a Charpy specimen obtained using backscattered electrons after chemical etching with V2A.

phase present at the grain boundaries and in early delta ferrite stringers is likely the sigma phase, whereas the smaller and whitish particles present inside the grains and at the grain boundaries likely correspond to a phase rich in molybdenum, possibly the Fe_2Mo type Laves phase (Table 1 and Figure 1).

The fracture surfaces of the Charpy specimens were observed under a SEM with backscattered and secondary electrons, as shown in Figures 4 and 5, respectively. The micrographs reveal granular microstructures with broad regions exhibiting brittle cleavage-type fracture interspersed with a few ductile dimples.

The second objective of this study was to identify the phase responsible for the cleavage-type fracture and low toughness measured in the Charpy test. Figure 6 presents the SEM image of the fracture surface and corresponding EDS analysis of the brittle phase.

Weiss and Stickler [8] and Weiss et al. [9] analyzed, with the aid of the SEM-EDS technique, the chemical composition of the phases present after aging in AISI 316 and 316L stainless steels and concluded that it is possible to identify the different phases in the steel microstructure (see Figure 7) based on the respective relationships (Mo/Cr) and (Fe/Cr). Table 3 presents the chemical composition of

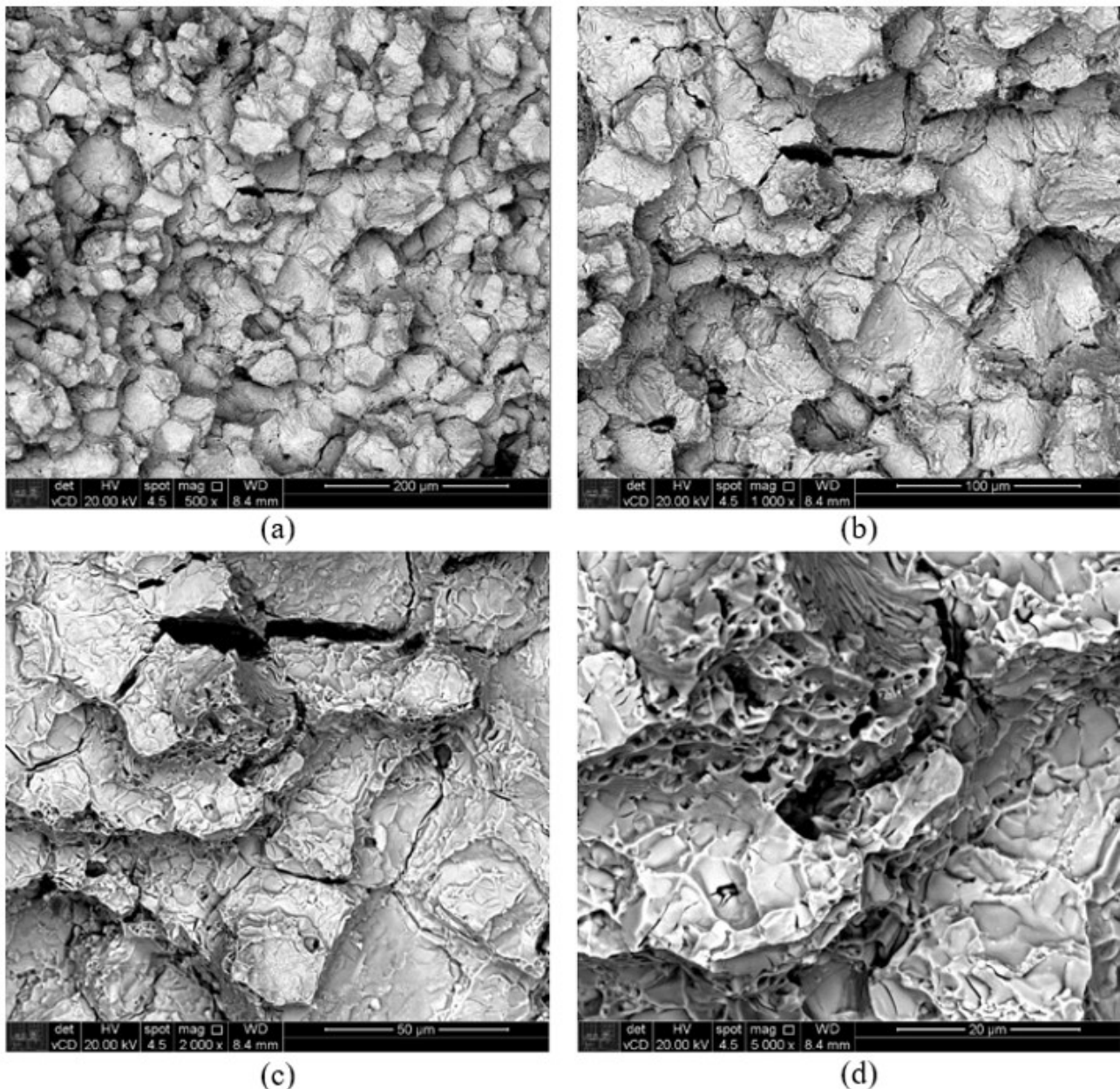


Figure 4. SEM images obtained using backscattered electrons at a) 500X, b) 1000X, c) 2000X, and d) 5000X.

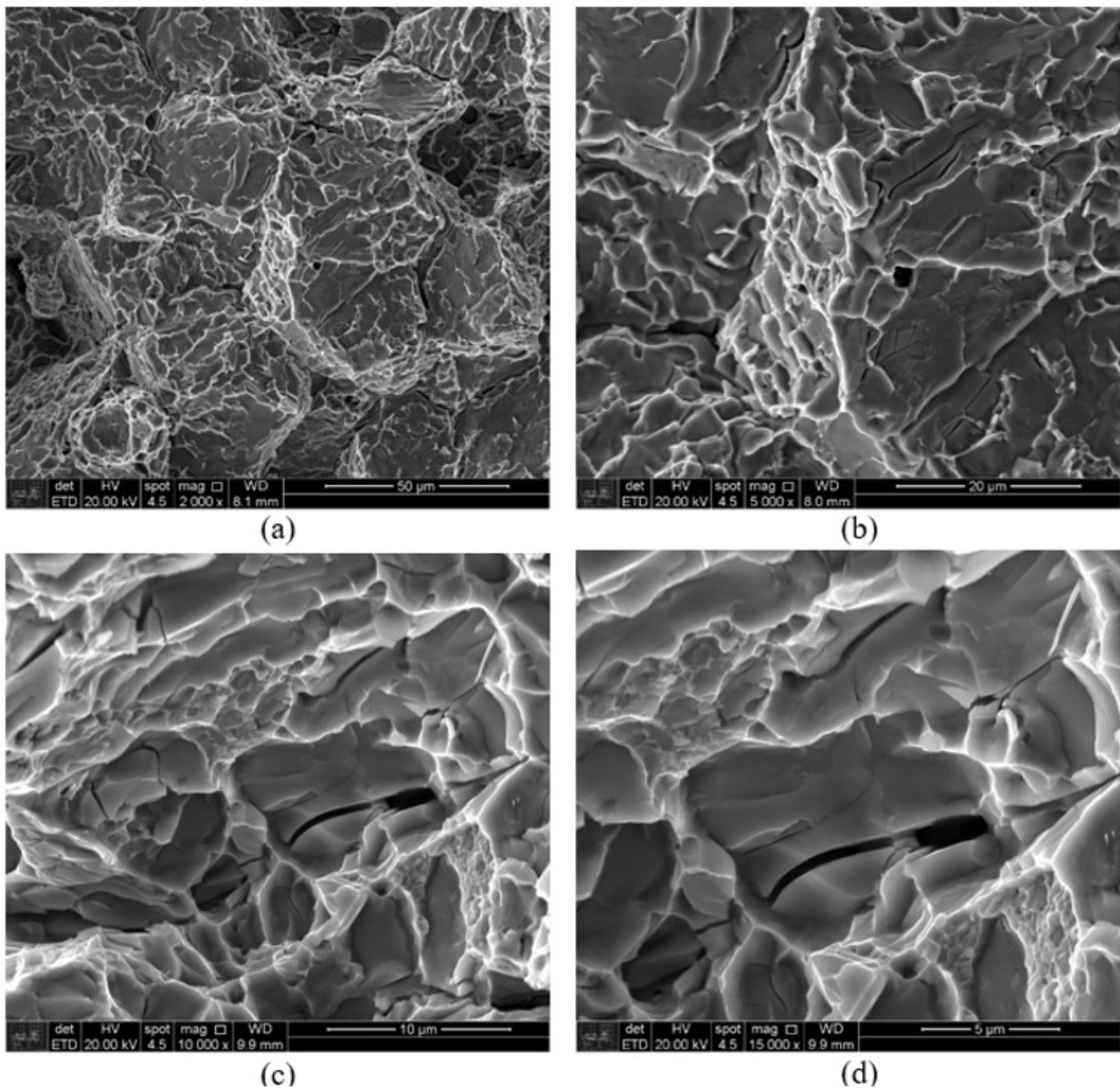


Figure 5. SEM images obtained using secondary electrons: a) 2000 X, b) 5000X, c) 10000X, and d) 15000X.

Table 3. Chemical composition (wt.%) of the brittle phase (see green rectangle in Figure 6a) determined by EDS

Phase/Element	Fe	Cr	Ni	Mo	Si	Mn	Fe/Cr	Mo/Cr
Brittle phase	53.43	30.67	4.57	8.82	1.04	1.47	1.74	0.288

the brittle phase shown in Figure 6. From Table 3, based on the criteria suggested by Weiss and Stickler [8] and Weiss et al. [9], the brittle phase can be considered as the sigma phase.

For 100,700 hours of exposure at 720 °C, the TTP diagram shown in Figure 1 suggests the presence of three

phases: $M_{23}C_6$, sigma, and Laves phases, with the presence of the Chi phase is considered uncertain. By contrast, analysis using the Thermo-Calc (TCFE10 database) program, presented in Figure 8, suggests the presence of four phases at 720 °C: $M_{23}C_6$, sigma (less than 0.03 volume fraction), Laves, and the nitride Cr_3Ni_2SiN (η).

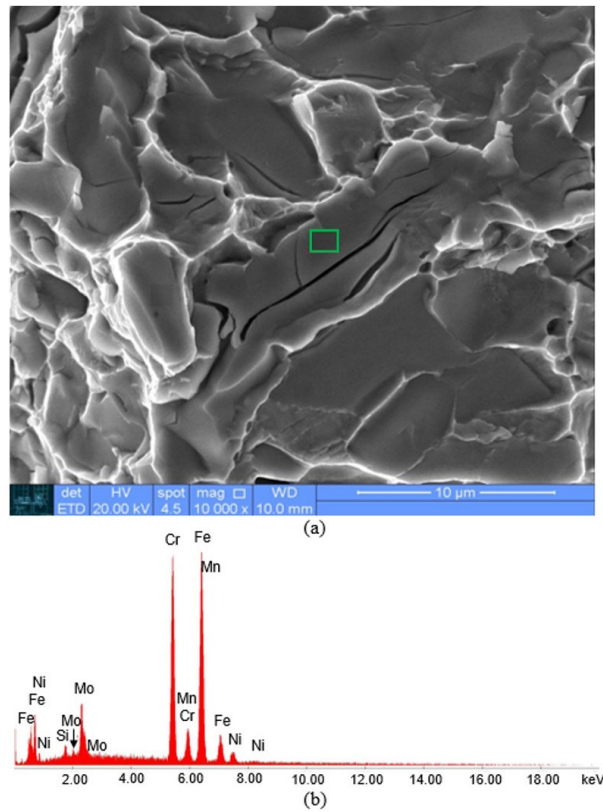


Figure 6. Analysis of the fracture surface with SEM/EDS: (a) SEM image obtained using secondary electrons and (b) EDS spectrum of the area inside the green rectangle marked in Figure 6a.

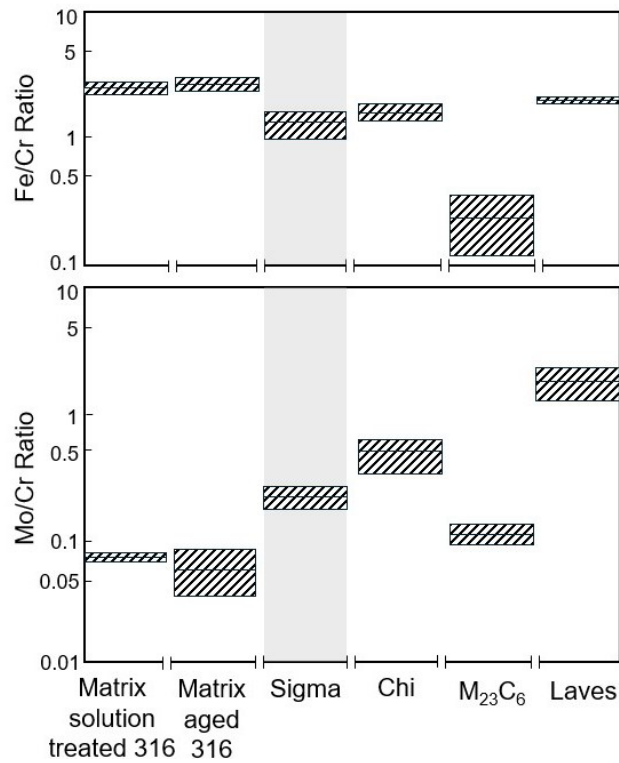


Figure 7. Intensity ratios of characteristic X-ray radiation obtained by energy-dispersive X-ray spectrometry of matrix and various phases in solution treated and aged type 316 austenitic stainless steel samples [9].

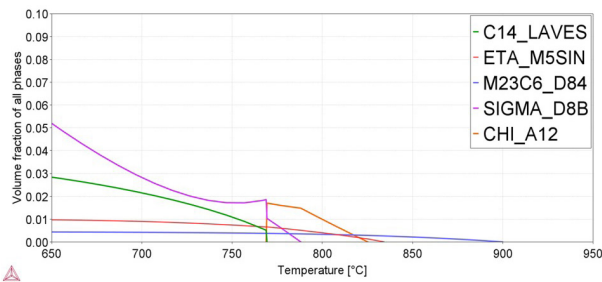


Figure 8. Variation in the percentage of phases as a function of temperature calculated using the Thermo-Calc computer program with TCFE10 database.

4 Conclusions

Although the TTT diagrams from the literature and predictions by the Thermo-Calc (TCFE10) program suggest the presence of multiple phases in the microstructure of the

investigated 316L steel, after exposure at 720 °C for 100,700 hours, the sigma phase precipitated at grain boundaries contributed significantly to the sharp drop in toughness as detected by Charpy tests. Other phases in the microstructure, including the sigma phase resulting from the eutectoid decomposition of delta ferrite, did not play a significant role in the observed decrease in toughness. The microstructural analysis conducted on the fracture surface was crucial in understanding the mode and mechanism of fracture, which was predominantly intergranular, caused by sigma phase cleavage.

Acknowledgements

The authors would like to thank CNPq (AFP/process number: 305051/2020-2) and CAPES (EMA/process numbers: 88887.631492/2021-00 and 88887.883845/2023-00) for granting scholarships.

References

- 1 Plaut RL, Herrera C, Escriba DM, Rios PR, Padilha AF. A short review on wrought austenitic stainless steels at high temperatures: processing, microstructure, properties and performance. *Materials Research*. 2007;10:453-460. <http://doi.org/10.1590/S1516-14392007000400021>.
- 2 Qin W, Li J, Liu Y, Kang J, Zhu L, Shu D, et al. Effects of grain size on tensile property and fracture morphology of 316L stainless steel. *Materials Letters*. 2019;254:116-119. <http://doi.org/10.1016/j.matlet.2019.07.058>.
- 3 Davis JR. *ASM Specialty Handbook: Stainless Steels*. Ohio: ASM International; 1994.
- 4 Moraes FP, Amaral EM, Neto FB, Padilha AF. Failure analysis of an AISI 316 steel pipe elbow exposed to the weather for three years after 16 years of operating at 515 °C. *Tecnologica em Metalurgia, Materiais e Mineração*. 2023;20:e2879. <http://doi.org/10.4322/2176-1523.20232879>.
- 5 Chopra OK. Effects of thermal aging and neutron irradiation on crack growth rate and fracture toughness of cast stainless steels and austenitic stainless steel welds. NUREG/CR-7185. ANL-14/10. USA: Nuclear Regulatory Commission, 2015.
- 6 Was GS. *Fundamentals of radiation materials science*. 2nd ed. Berlin/Heidelberg: Springer-Verlag GmbH; 2017. Chapter 14: Fracture and Embrittlement. pp. 793-856.
- 7 Griffiths M. Effect of neutron irradiation on the mechanical properties, swelling and creep of austenitic stainless steels. *Materials (Basel)*. 2021;14(10):2622. <http://doi.org/10.3390/ma14102622>.
- 8 Weiss B, Stickler R. Phase instabilities during high temperature exposure of 316 austenitic stainless steel. *Metallurgical and Materials Transactions. B, Process Metallurgy and Materials Processing Science*. 1972;3:851-866.
- 9 Weiss B, Hughes CW, Stickler R. SEM-Techniques for microcharacterization of metals and alloys II. *Practical Metallography*. 1971;8(9):528-542.
- 10 Lai JKL. A study of precipitation in AISI type 316 stainless steel. *Materials Science and Engineering*. 1983;58(2):195-209. [http://doi.org/10.1016/0025-5416\(83\)90046-0](http://doi.org/10.1016/0025-5416(83)90046-0).
- 11 Minami Y, Kimura H, Ihara Y. Microstructural changes in austenitic stainless steels during long-term aging. *Materials Science and Technology*. 1986;2(8):795-806. <http://doi.org/10.1179/mst.1986.2.8.795>.
- 12 Padilha AF, Rios PR. Decomposition of austenite in austenitic stainless steel. *ISIJ International*. 2002;42(4):325-327. <http://doi.org/10.2355/isijinternational.42.325>.
- 13 Padilha AF, Escriba DM, Materna-Morris E, Rieth M, Klimenkov M. Precipitation in AISI 316L(N) during creep tests at 550 and 600 °C up to 10 years. *Journal of Nuclear Materials*. 2007;362:132-138. <http://doi.org/10.1016/j.jnucmat.2006.12.027>.

- 14 Moraes FP, Alves SF Jr, Plaut RL, Padilha AF. Degradation of microstructure and properties of an AISI 316L steel pipe after more than 100,000 hours usage at 640 °C in a petrochemical industry. *Procedia Structural Integrity*. 2019;17:131-137. <http://doi.org/10.1016/j.prostr.2019.08.018>.
- 15 National Institute of Materials Science. Creep data sheet: metallographic atlas of long-term crept materials, no. M-2: micrographs and microstructural characteristics of crept specimens of 18Cr-12Ni-Mo stainless steel for boiler and heat exchanger seamless tubes (SUS 316H TB). Japan: NIMS; 2003.
- 16 Sourmail T. Precipitation in creep resistant austenitic stainless steels. *Materials Science and Technology*. 2001;17:1-14. <http://doi.org/10.1179/026708301101508972>.
- 17 Rios PR, Padilha AF. Precipitation from austenite. In: Hashmi S, editor, *Reference module in materials science and materials engineering*. Oxford: Elsevier; 2019. pp. 1-8.
- 18 Johansson C, Lind M. Evaluation of the η (Eta) nitride with three laboratory melts [thesis]. Stockholm, Sweden: KTH; 2015.
- 19 Maziasz PJ. The formation of diamond-cubic eta phase in type 316 stainless steel exposed to thermal aging or irradiation environments. *Scripta Metallurgica*. 1979;13:621-626. [http://doi.org/10.1016/0036-9748\(79\)90121-2](http://doi.org/10.1016/0036-9748(79)90121-2).
- 20 Martorano MA, Tavares CF, Padilha AF. Predicting delta ferrite content in stainless steel castings. *ISIJ International*. 2012;52(6):1054-1065. <http://doi.org/10.2355/isijinternational.52.1054>.
- 21 Santos FAM, Martorano MA, Padilha AF. Delta ferrite formation and evolution during slab processing from an 80-ton industrial heat of AISI 304 austenitic stainless steel. *REM - International Engineering Journal*. 2023;76(1):47-54. <http://doi.org/10.1590/0370-44672022760001>.
- 22 Benes L. Correlation between chemical compositions and ferrite contents of austenitic stainless steels. *Metalurgia-Bucharest*. 1978;30(8):467-469.
- 23 Neidel A, Fischer B, Rienbeck S, Cagliyan E. Transformation of delta ferrite into sigma-phase in metastable austenitic stainless steels after long-term high-temperature service exposure. *Practical Metallography*. 2014;51(4):259-279. <http://doi.org/10.3139/147.110278>.
- 24 Wang Q, Chen S, Rong L. δ -Ferrite formation and its effect on the mechanical properties of heavy-section AISI 316 stainless steel. *Metallurgical and Materials Transactions. A, Physical Metallurgy and Materials Science*. 2020;51A:2998-3008. <http://doi.org/10.1007/s11661-020-05717-0>.
- 25 Petzow G. *Metallographic etching*. Metals Park, Ohio, USA: American Society for Metals; 1978.

Received: 09 Feb. 2024

Accepted: 07 July 2024